Effects of Fusion Zone Size on Failure Modes and Static Strength of Aluminum Resistance Spot Welds

A larger weld size creates a higher level of peak load and energy absorption

BY X. SUN, E. V. STEPHENS, R. W. DAVIES, M. A. KHALEEL, AND D. J. SPINELLA

ABSTRACT. This paper examines the effects of fusion zone size on failure modes, static strength, and energy absorption of aluminum spot welded samples using a combined experimental, statistical, and analytical approach. The main failure modes for aluminum spot welds are nugget pullout and interfacial fracture. First, static strength tests using coupon configurations of lap shear, cross tension, and coach peel were performed on the joint populations with a controlled fusion zone size. Thirty replicate static strength tests were performed for each coupon configuration. The resulting peak load and energy absorption levels associated with each failure mode were studied using statistical models. Next, an analytical model was developed to determine the failure mode of an aluminum resistance spot weld based on limit load analyses. It was found that fusion zone size, sheet thickness, and the level and location of weld porosity/defects are the main factors influencing the cross-tension failure mode of an aluminum spot weld. Two additional spot weld populations with different fusion zone sizes were then fabricated to validate the analytical failure mode model. Static cross-tension tests were again performed, and the experimental observations confirmed the analytically predicted failure modes for each population.

Introduction

Resistance spot welding (RSW) has been used for decades by automotive and other industries for fabricating sheet metal assemblies. Resistance spot welding is easy to operate, automate, control, and perform, and thus is an ideal joining technology for mass production. Over the years, RSW technology has been perfected for various steel grades and sheet metal thicknesses to deliver high-quality, durable structural joints (Refs. 1–3). Recently, because of their light weight and relatively high strength, more and more aluminum alloys have been used in the construction of automobile body and panel parts to reduce weight and therefore enhance fuel efficiency. As one of the primary joining methods in the automotive industry, the RSW process for aluminum alloys has been studied intensively over the past two decades (Refs. 4–8).

Spot welding of aluminum alloys shares the same overall Joule heating principle as spot welding of steel. However, because of the relatively low density and high thermal and electrical conductivity of aluminum alloys, aluminum spot welding also presents some unique challenges to the automotive industry. Higher welding currents, typically two to three times those of steel, and only one-third of the welding duration are used. The issues associated with production welding of aluminum alloys include weld porosity, weld expulsion, electrode wear, and inconsistency in failure mode during coupon-level joint quality evaluation (Refs. 17, 18).

As a means of quality control, the domestic automotive industry historically has adopted an approach and criterion for aluminum spot welds similar to those used in spot welds of mild steel; that is, a peel test to determine whether a satisfactory weld has been produced. The common criterion is borrowed from the conventional spot weld criterion for mild steel, in which the minimum weld button diameter (D) should be equal to or larger than $4\sqrt{t}$ (t defined as material thickness in mm) (Ref. 9). Undersized welds have an average weld button diameter larger than $2\sqrt{t}$, but less than $4\sqrt{t}$. Defective welds have average weld button diameters less than or equal to $2\sqrt{t}$. Any weld that fails in the interfacial fracture mode would be considered a "bad" weld and would be rejected by the quality control inspector.

This criterion works relatively well for mild steel spot welds because the weld nugget has a significantly higher hardness level (therefore yield strength) than the base material; hence, the nugget pullout mode would produce the highest joint strength. On the other hand, the effectiveness of this criterion for the quality evaluation of aluminum spot welds and advanced high-strength steel spot welds has not been adequately studied by the automotive welding community; it was adopted from mild steel spot welds without much in-depth study. Because of the more frequent occurrence of interfacial fracture, many domestic automotive companies do not have confidence in aluminum spot welds and are now pursuing alternative, yet more expensive, joining techniques such as riveting and/or clinching.

The purpose of this paper is to study the effects of fusion zone size and failure modes on the peak load and energy absorption levels of aluminum spot welds. First, two sample weld populations were considered:

1) Weld population ID14: RSW of 2-mm 5182-O to 2-mm 5182-O

2) Weld population ID15: RSW of 2-mm 5182-O to 2-mm 6111-T4.

For each weld population, three coupon configurations were included in the static tests: lap shear, cross tension, and coach peel. See Figs. 1–3 for specimen design, dimensions, and fixture design. For each static test, a load vs. displacement curve was recorded, as were the failure mode and nugget size/fusion zone size of the joint sample. The total energy absorption, which is represented by the area under the load vs. displacement curve, was then calculated through numerical integration. Thirty identical static strength tests were performed for each joint con-

KEY WORDS

Resistance Spot Welding
Aluminum Sheet Metal
Fusion Zone Size
Weld Failure Modes
Coach Peel Test
Lap Shear Test
Cross-Tension Test
Weibull Distribution

X. SUN, E. V. STEPHENS, R. W. DAVIES, and M. A. KHALEEL are with Pacific Northwest National Laboratory, Richland, Wash. D. J. SPINELLA is with Alcoa Technical Center, Alcoa Center, Pa.

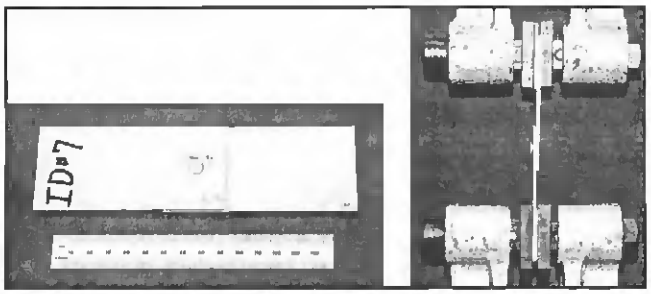

Fig. 1 — Lap-shear coupon design and test fixture.

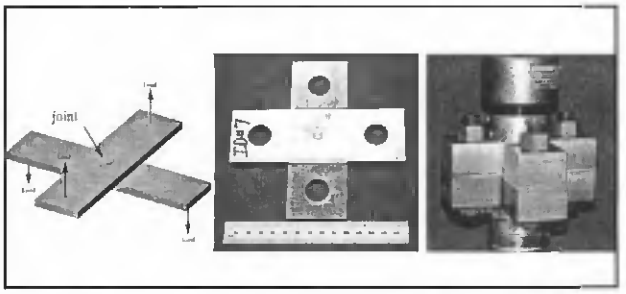

Fig. 2 — Cross-tension coupon design and test fixture.

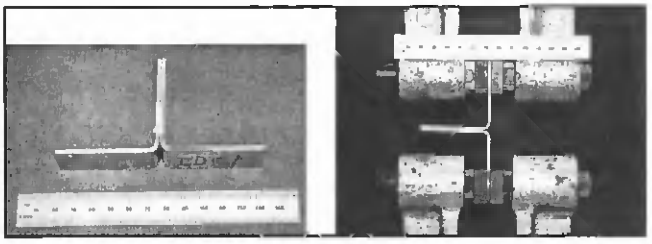

Fig. 3 — Coach peel coupon design and fixture.

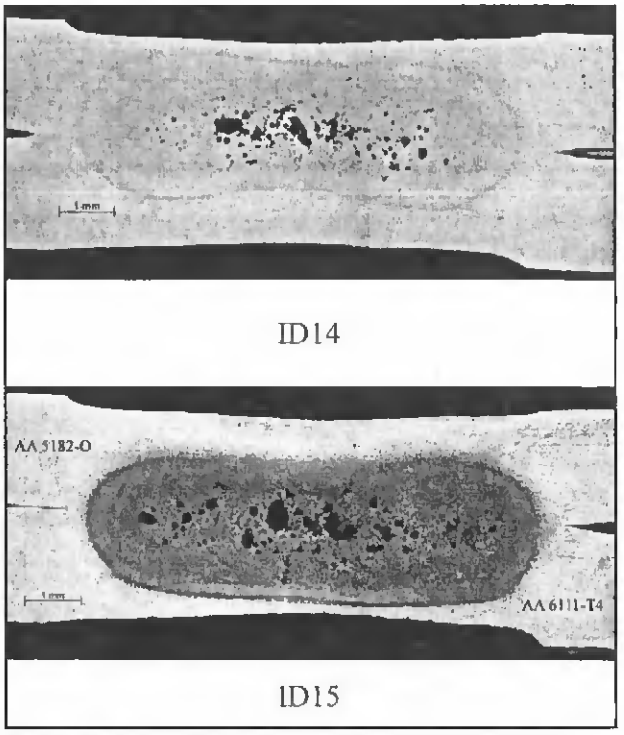

Fig. 4 — Typical metallurgical cross sections for ID14 and ID15.

figuration, and statistical analyses were performed to study the effects of different failure modes on the peak load and energy absorption of the weld joints.

Next, a simple, limit-load-based analytical model was derived to rationalize the experimental observed failure modes for aluminum spot welds with the aid of microhardness measurements of the weld samples. Two additional weld populations with different fusion zone sizes were then fabricated and tested to validate the analytical model. The goal of this study is to provide welding engineers with some insights on the anticipated joint failure modes for a given weld population with certain weld attributes, and to discuss the effects of weld size and weld porosity (irregularity) level on the anticipated levels of weld strength and failure mode.

Experimental Study

The initial experimental work in this investigation consisted of quasistatic tests of lap shear, coach peel, and cross tension of ID14 and ID15. The specimen and test fixture designs are shown in Figs. 1–3. The RSW specimens were fabricated at the Alcoa Technical Center. The following welding parameters were used in the coupon fabrication process:

Electrodes: 0.370-in. face diameter truncated electrode
Current: ~34.0 kA, 80% current, AC welding machine
Force: 1050 lbf
Weld time: 8 cycles
Water flow rate: 2.6 gal/min.

Special efforts were made to ensure that the location of the welds was in the width center of the specimens. Electrode tips were dressed every 15 welds to ensure weld consistency. Peel tests and metallographic cross sections were used to maintain a nugget diameter of ~8 mm for all specimens. Figure 4 shows the typical weld metallurgical cross sections for ID14 and ID15, respectively.

Quasistatic tests at a rate of 10 mm/min were performed on these specimens to determine their load vs. displacement curves. Figure 5 shows the typical experimental results for ID14 under the three loading configurations. Thirty static tests were performed for each joint population and each loading configuration. Tables 1–6 tabulate the test results with peak load, failure mode, and energy absorption for each population and each loading configuration. Nomenclatures used in defining different failure modes are also included at the end of Table 1.

Lap Shear Tests

For lap shear samples of both populations ID14 and ID15, interfacial fracture was the only failure mode observed. The average peak failure load for ID14 was 7.16 kN, and the average peak failure load for ID15 was 7.17 kN, with no significant amount of sheet bending deformation observed for either population.

Cross-Tension Tests

Both nugget pullout and interfacial fracture modes were observed for the cross-tension samples of ID14 and ID15, and the majority of the samples failed in pullout mode. The average peak loads were 6.05 and 5.95 kN for ID14 and ID15, respectively. A detailed statistical analysis will be presented in the next section to study whether different failure modes have a significant influence on the peak failure loads for these two populations.

Coach Peel Tests

Similar to the cross-tension samples, the failure modes for coach peel samples were also a combination of nugget pullout and interfacial fracture. However, in coach peel samples, interfacial fracture and partial interfacial fracture (a combination of interfacial fracture and later stage nugget pullout) were more often ob-

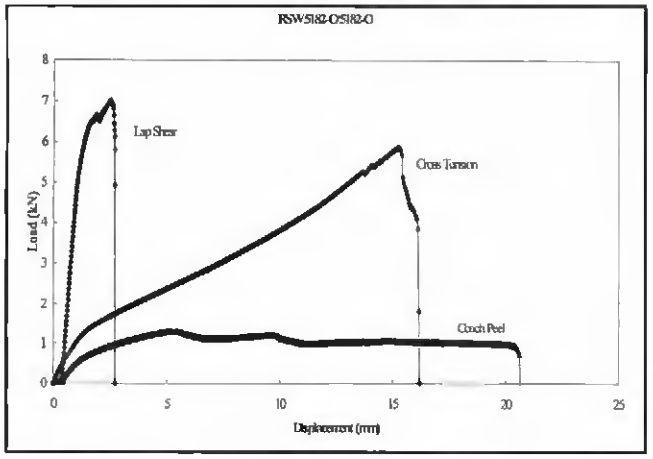

Fig. 5 — Sample load vs. displacement curves for ID14.

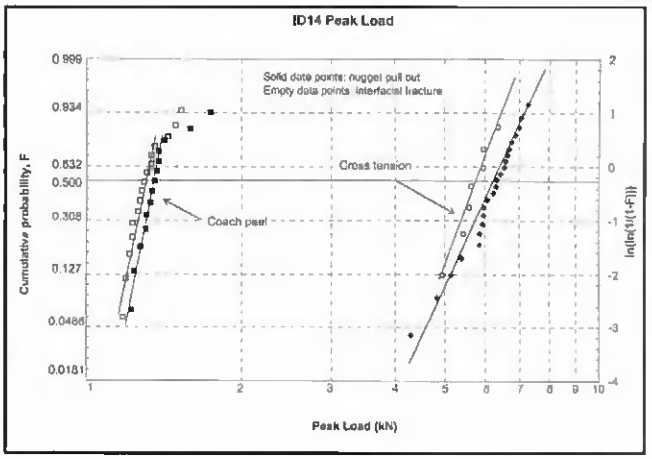

Fig. 6 — Weibull distribution comparing ID14 peak load distribution for interfacial fracture and pullout modes.

Table 1 — ID14 Lap-Shear Data Summary

Specimen	Peak Load (kN)	Energy (Nmm)	Failure Mode
	Lap Shear		
Joint ID 14 (RSW): 5182-0/5182-0 (2 mm/2 mm)			
14LC-1	7.02	13,129.72	IF
14LC-2	7.11	10,593.42	IF
14LC-3	6.99	12,426.27	IF
14LC-4	7.64	11,488.31	IF
14LC-5	6.94	13,150.59	IF
14LC-6	6.85	13,335.88	IF
14LC-7	7.47	15,783.62	IF
14LC-8	7.01	10,527.91	IF
14LC-9	7.46	12,049.34	IF
14LC-10	7.26	13,252.42	IF
14LC-11	6.98	11,183.65	IF
14LC-12	7.07	13,468.99	IF
14LC-13	7.39	12,633.53	IF
14LC-14	7.68	17,064.19	IF
14LC-15	7.42	12,962.75	IF
14LC-16	7.17	13,755.13	IF
14LC-17	6.94	11,573.09	IF
14LC-18	6.82	10,365.50	IF
14LC-19	7.18	15,986.13	IF
14LC-20	7.28	17,896.04	IF
14LC-21	7.25	16,505.36	IF
14LC-22	7.29	13,025.95	IF
14LC-23	6.94	13,090.24	IF
14LC-24	7.33	13,329.21	IF
14LC-25	6.93	8,814.00	IF
14LC-26	7.30	9,416.71	IF
14LC-27	6.95	8,235.89	IF
14LC-28	7.06	10,552.38	IF
14LC-29	7.34	9,396.98	IF
14LC-30	7.15	9,101.55	IF
Maximum	7.68	17,896.04	
Mean	7.17	12,469.83	
Minimum	6.82	8,235.89	

Nomenclature throughout Tables 1–8:
IF: Interfacial fracture
PO: Nugget pullout
SS: Sheet shearing
PO-IF: Pullout is primary failure mode; interfacial fracture is secondary failure mode

served. In some samples, sheet tearing failure was also observed after nugget pullout, which increased the energy absorption levels of those samples significantly. Again, a statistical analysis will be conducted for the coach peel samples, and discussions in the next section will reveal whether different failure modes have a significant impact on the peak load and energy absorption levels of these two populations.

Statistical Data Analysis

Probability Paper and Weibull Distribution

The statistical characteristics of a data set can be analyzed with some mathematical tools such as a probability paper (Refs. 10–11). Following specific mathematical procedures, if all the data points in a data set plot approximately on a straight line on a certain probability paper, the distribution corresponding to that paper may be an appropriate distribution model for the data population under examination. Moreover, the characteristics of the line fitting the data on the probability paper will quantify the mean value and standard deviation of the data population according to the specific distribution type.

In studying the statistical nature of spot weld strength under different loading conditions, the static strength and energy absorption for different failure modes are analyzed using the two-parameter Weibull distribution:

$$F = 1 - \exp\left[-\left(\frac{\sigma}{\sigma_0}\right)^m\right] \qquad (1)$$

in which F denotes median estimator of the cumulative failure probability and is given by $F = (i - 0.3)/(N + 0.4)$, where i is the ranking of each specimen with values 1, 2, ... N and N is the total number of specimens, σ is the peak load (or energy absorption), and σ_0 and m are Weibull parameters. Physically, as may be verified from Equation 1, σ_0 is the peak load (or energy) value corresponding to a failure probability of 63.2%, and m is the slope of $\ln \ln[1/(1 - F)]$ vs. $\ln \sigma$ plot, otherwise known as Weibull modulus, or shape parameter (Ref. 11). For a unimodal distribution, m is analogous to the inverse of the standard deviation expressed as a fraction of mean strength. Therefore, the more vertical the data line is on a $\ln \ln[1/(1 - F)]$ vs. $\ln \sigma$ plot (or Weibull plot), the higher the value m, and the less scattered the data are in a statistical sense.

Construction of Weibull Plots

To study the effects of different failure modes on the peak load and energy absorption for the weld samples in ID14 and ID15, we took the static test results listed in Tables 2, 3, 5, and 6 and categorized them into two subpopulations based on individual samples' failure modes, namely, nugget pullout failure and interfacial fracture failure. The data points within each subpopulation were then sorted in ascending order in terms of peak load or energy absorption in order to be plotted on Weibull probability paper (Ref. 10). Figures 6 and 8 show the Weibull plots of peak load for ID14 and ID15, respectively, and Figs. 7 and 9 show the Weibull plots of energy absorption levels for ID14 and ID15, respectively. It should be noted that the cases with partial interfacial fracture were grouped as interfacial fracture based on their primary failure modes.

Assuming the available data points in each subpopulation of different failure modes are sufficient for statistical significance, the characteristics of the Weibull plots for interfacial fracture and nugget

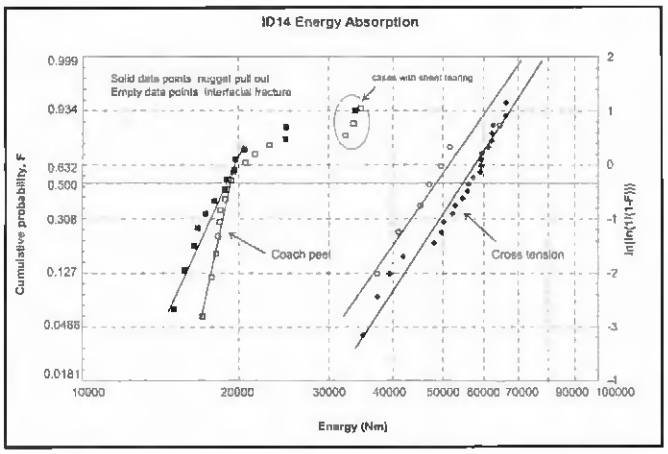

Fig. 7 — Weibull distribution comparing ID14 energy absorption for interfacial fracture and pullout modes.

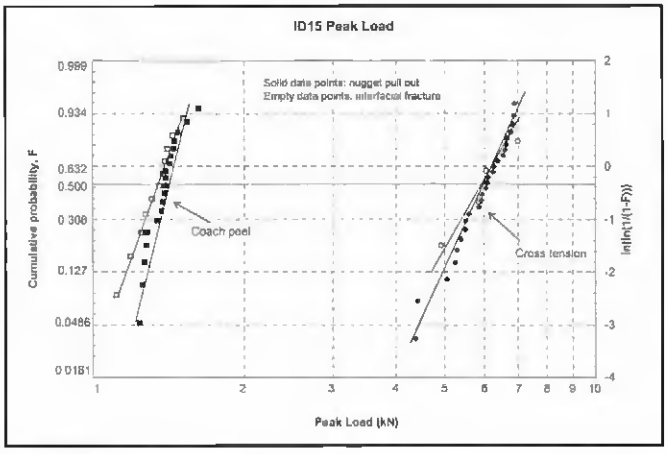

Fig. 8 — Weibull distribution comparing ID15 peak load distribution for interfacial fracture and pullout modes.

pullout modes can provide the median value as well as the degree of scatter for each failure mode. It should be noted that since interfacial fracture was the only failure mode observed for all the lap shear samples of ID14 and ID15, no statistical study was performed on the data listed in Tables 1 and 4.

Cross Tension

The linearity of curve fittings for pullout and interfacial fracture failure modes in Figs. 6–9 suggests that the peak load and energy distribution under cross tension for ID14 and ID15 can be modeled approximately with Weibull distributions with different shape parameters.

For ID14 under cross tension, the Weibull plots in Fig. 6 show that the median peak load for interfacial fracture is about 10% lower than the median peak load for pullout failure. Consistently, the median energy absorption for interfacial fracture is about 10% lower than that of pullout mode for this population. Since the fitted straight lines in Fig. 6 are almost parallel, it is concluded that the interfacial fracture and pullout failure modes have the same shape parameters for Weibull distribution, and therefore the degree of peak load and energy scatter is about the same for these two failure modes for ID14.

For ID15 under cross tension, the Weibull plots in Fig. 8 show that the median peak load levels for the two failure modes are almost identical. However, the interfacial fracture mode shows a higher level of scatter on peak load than the pullout mode. Similar observations can be made for the energy absorption levels for the two failure modes for ID15 under cross tension — Fig. 9.

Coach Peel

Under coach peel loading configuration, the lack of linearity of the data points for ID14 and ID15 indicates that a unimodal Weibull distribution cannot be used to correctly model the entire data population — Figs. 6–9. However, the few cases in the peak load distributions that do not fit on the straight lines are mostly the cases with combined failure modes of nugget pullout and sheet tearing. If we were to consider the majority cases represented by the straight lines, consistent conclusions on peak load distributions under the coach peel condition can again be reached for the two weld populations as those under cross tension: the median peak load for interfacial fracture mode is lower than that for the nugget pullout mode. But the median value difference for the two failure modes is less than 10%.

The distributions for energy absorption under coach peel loading conditions for ID14 and ID15 have a bilinear nature. Therefore, bimodal Weibull distributions may be more suitable for these energy distributions. In Fig. 7, the cases with sheet tearing have distinguishable higher energy levels due to the additional energy absorbed by base metal tearing deformation.

In conclusion, the above statistical analyses indicate that the median peak load for the cases that failed in interfacial fracture mode is about 10% lower than that of the cases that failed in pullout mode for ID14, and that the median peak load is about the same for ID15 with different shape parameters. Similar conclusions can also be reached for the energy absorption levels. These results indicate that, for weld populations ID14 and ID15, the differences in failure modes under cross-tension and coach peel conditions do not produce a significant difference in the specimens' peak load and energy absorption levels. Nugget pullout mode only produces slightly higher peak load and energy absorption.

It should also be noted that, in general,

Table 2 — ID14 Cross-Tension Data Summary

Specimen	Cross Tension Peak Load (kN)	Cross Tension Energy (Nmm)	Cross Tension Failure Mode
Joint ID 14 (RSW): 5182-O/5182-O (2 mm/2 mm)			
14TC-1	5.58	40,970.85	IF
14TC-2	6.88	62,010.95	PO
14TC-3	5.95	49,615.49	PO
14TC-4	6.63	62,404.24	PO
14TC-5	6.23	54,467.28	PO
14TC-6	6.05	50,141.73	PO
14TC-7	6.57	59,254.26	PO
14TC-8	6.99	66,002.44	PO
14TC-9	5.95	51,533.12	IF-PO
14TC-10	4.82	37,281.09	PO
14TC-11	6.43	59,179.87	PO
14TC-12	5.83	52,073.55	PO
14TC-13	6.68	59,364.00	PO
14TC-14	5.43	45,128.99	IF-PO
14TC-15	4.93	37,263.02	IF-PO
14TC-16	5.92	48,008.35	PO
14TC-17	5.62	49,457.98	IF-PO
14TC-18	4.28	34,930.96	PO
14TC-19	5.13	39,341.73	PO
14TC-20	6.31	55,954.47	PO
14TC-21	6.35	64,342.24	IF-PO
14TC-22	5.86	52,734.13	PO
14TC-23	7.26	66,047.73	PO
14TC-24	6.75	62,165.33	PO
14TC-25	5.96	57,083.67	PO
14TC-26	6.54	59,019.29	PO
14TC-27	6.28	55,635.41	PO
14TC-28	5.38	41,779.10	PO
14TC-29	5.94	46,972.13	IF-PO
14TC-30	7.06	61,131.00	PO
Maximum	7.26	66,047.73	
Mean	6.05	52,709.81	
Minimum	4.28	34,930.96	

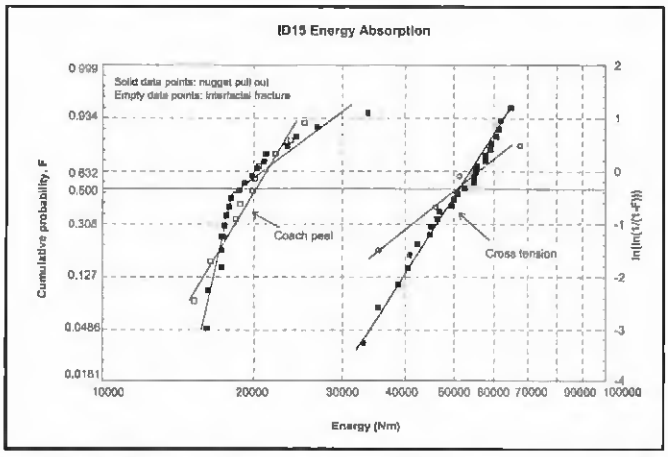

Fig. 9 — Weibull distribution comparing ID15 energy absorption for interfacial fracture and pullout modes..

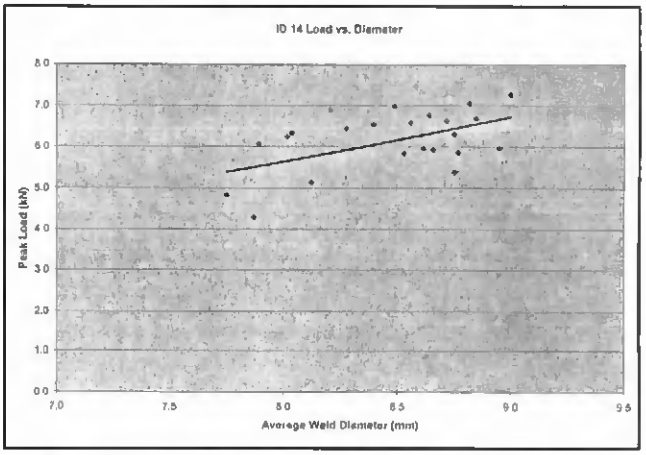

Fig. 10 — ID14 cross-tension peak load vs. average weld diameter.

Table 3 — ID14 Coach-Peel Data Summary

Specimen	Peak Load (kN)	Energy (Nmm)	Failure Mode
	Coach Peel		
Joint ID 14 (RSW): 5182-O/5182-O (2 mm/2 mm)			
14CC-1	1.33	17,248.00	PO
14CC-2	1.28	34,647.00	IF-PO-SS
14CC-3	1.36	17,728.00	IF-PO
14CC-4	1.74	33,756.00	PO-SS
14CC-5	1.23	19,376.00	IF-PO
14CC-6	1.18	23,001.00	IF-PO
14CC-7	1.31	21,564.00	IF-PO
14CC-8	1.27	17,922.00	PO
14CC-9	1.34	18,950.00	PO
14CC-10	1.49	18,260.00	IF-PO
14CC-11	1.44	19,590.00	IF-PO
14CC-12	1.38	16,662.00	PO
14CC-13	1.35	19,612.00	PO
14CC-14	1.30	18,776.00	PO
14CC-15	1.19	18,089.00	IF-PO
14CC-16	1.22	15,726.00	PO
14CC-17	1.52	18,857.00	IF-PO
14CC-18	1.30	24,785.00	PO
14CC-19	1.23	18,405.00	IF-PO
14CC-20	1.37	24,752.00	PO-SS
14CC-21	1.26	33,514.00	IF-PO-SS
14CC-22	1.29	20,649.00	IF-PO
14CC-23	1.27	17,007.00	IF-PO
14CC-24	1.38	16,411.00	PO
14CC-25	1.24	15,026.00	PO
14CC-26	1.33	18,996.00	IF-PO
14CC-27	1.34	18,449.00	IF-PO
14CC-28	1.59	20,558.00	PO
14CC-29	1.21	32,406.00	IF-PO-SS
14CC-30	1.42	19,766.00	PO
Maximum	1.74	34,647.00	
Mean	1.34	21,016.27	
Minimum	1.18	15,026.00	

the estimator F should be selected carefully according to the circumstances in the Weibull analysis. In studying our test data, we have also tried using two other types of estimators, i.e., $F = i/(N + 1)$ and $F = (i - 0.5)/N$, and the resulting data distribution characteristics do not change significantly.

Influence of Weld Size on Peak Load and Energy Absorption

To examine the relationships between weld size vs. peak load and weld size vs. energy absorption for ID14 and ID15 under cross tension, the minimum and maximum nugget diameters were measured for all the cross-tension samples that failed in pullout mode, and the average nugget diameters were then calculated. Next, for each population, a scatter plot of peak load and energy vs. weld size was constructed, and a trend line was added to the scatter plot to show the general relationship — Figs. 10–13. Although the data in these plots are quite scattered, the trend lines indicate that there is a general linear relationship between weld size vs. peak load and weld size vs. energy absorption. The linear relationship suggests that, within a weld population, a larger weld generates higher peak load and higher energy absorption.

Analytical Failure Mode Prediction for Aluminum Spot Welds under Cross-Tension Loading Condition

In this section, we will attempt to derive a simple, limit-load-based analytical strength model to predict joint strength and the associated failure mode for an aluminum spot weld under static cross-tension loading. As shown in Fig. 4, a typical cross section of an aluminum spot weld consists of base metal, weld nugget, and the region between the base metal and the nugget: the heat-affected zone (HAZ). Let us denote the weld fusion zone diameter as D, the sheet thickness on the thinner side as t, and assume that the weld has a porosity factor f, which is defined as

$$f = \frac{A_{total} - A_{porosity}}{A_{total}}, \quad 0 < f \le 1.0 \qquad (2)$$

In Equation 2, A_{total} is the total area of the fusion zone on the faying interface, and $A_{porosity}$ is the projected area of porosity in the fusion zone on the faying interface of the weld. The factor f is defined in such a way that a porosity-free weld has an f value equal to 1.0, and a weld that has some degree of porosity on the faying interface has an f value less than 1.0, but greater than 0. We assume that porosity does not concentrate at the weld periphery, such that the existence of porosities does not affect the local stress distribution around the weld tip and therefore would not influence the local crack growth path for the weld under static cross-tension loading.

It should be mentioned that the location of porosity within an aluminum spot weld is a topic that attracts the attention of many researchers. Our assumption here that porosities do not locate at the weld periphery is first supported by the typical cross sections of welds in ID14 and ID15 as shown in Fig. 4. Furthermore, the experimental studies by Chuko and Gould (Ref. 18) revealed that weld porosity at the nugget edge faying interface held constant at less than 1% and away from the fusion zone periphery for the first 200 spot welds of 1-mm AA5754 sheet with chromate-based coating. Chuko and Gould (Ref. 18) also reported a sharp increase of weld porosity at the nugget edge on faying interface (of up to

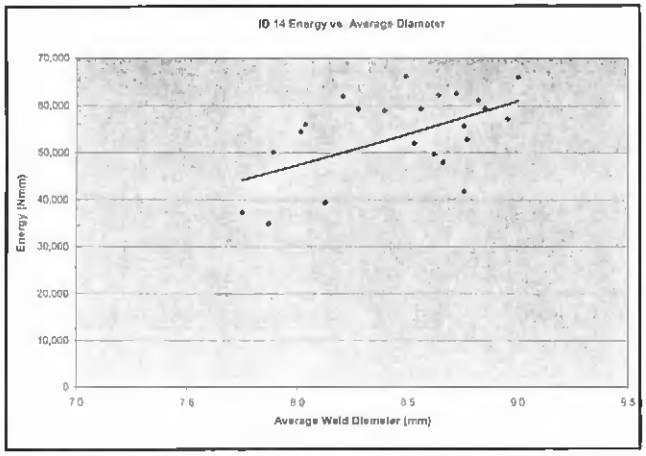

Fig. 11 — ID14 cross-tension energy absorption vs. average weld diameter.

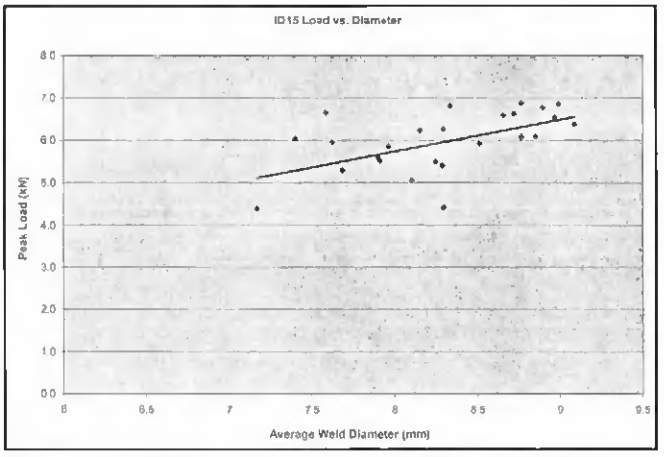

Fig. 12 — ID15 cross-tension peak load vs. average weld diameter.

9%) for the 200th and 300th welds during their electrode life study. Since we do not address the effects of electrode wear on joint strength and failure mode in this study, our assumption on porosity location for the welds made with fresh electrodes should be sufficient.

Assuming axisymmetric deformation under the cross tension loading condition, the peak load for a weld to fail in interfacial fracture mode can be approximated as

$$F_{IF} = f \cdot A_{total} \cdot \sigma_{y-weld} = f \cdot \pi \cdot \frac{D^2}{4} \cdot \sigma_{y-weld} \qquad (3)$$

where $\sigma_{y\text{-}weld}$ represents the tensile yield strength of the weld metal. We use tensile yield strength of the weld metal instead of ultimate strength because this is a limit load analysis in which no local material hardening or necking is considered (Ref. 13).

On the other hand, if the spot welds fail in nugget pullout mode, experiments have shown that failure normally occurs by through-thickness shear in the heat-affected zone (Ref. 13). Therefore, the peak load for a weld to fail in nugget pullout mode under cross tension can be approximated as

$$F_{PO} = \pi \cdot D \cdot t \cdot \sigma_{y-HAZ-shear} \qquad (4)$$

In Equation 4, $\sigma_{y-HAZ-shear}$ represents the shear yield strength of the heat-affected zone. Again, this is a limit load estimation in which yield strength is used instead of ultimate strength because no necking or material hardening in the heat-affected zone are considered. It should be mentioned that Equation 4 also assumes no significant weld indentation. If noticeable weld indentation occurs from the welding process, a reduced level of t should be used, based on the actual residual sheet thickness around the weld periphery.

The failure mode of a specific weld under cross-tension loading condition can then be determined by selecting the failure mode associated with the lower peak load level according to Equations 3 and 4, given the values of σ_{y-weld} and $\sigma_{y-HAZ-shear}$. In principle, this methodology should apply for both steel and aluminum spot welds. Here we use aluminum spot welds as an example.

In order to ensure pullout failure for an aluminum spot weld, the following inequality needs to be satisfied:

$$F_{PO} < F_{IF} \qquad (5)$$

Figure 14 shows the microhardness traverse for a typical weld in ID14. Figure 15 shows the line plot of hardness measurement of a typical weld in ID15. The hardness data shown in Figs. 14 and 15 indicate that the difference in the hardness of the base metal and the weld metal is not significant. Consequently, we can deduce that the tensile yield strength of the weld nugget for an aluminum weld should be close to that of the base metal. The average hardness level of the HAZ is about 15% higher than the average hardness of the base metal. These microhardness observations for aluminum RSW are in contrast with those for mild steel RSW in which the weld nugget and the HAZ have much higher hardness values than the base metal (Ref. 14).

Since a material's tensile yield strength can be considered linearly related to its hardness level (Ref. 14), the tensile yield strength of the weld metal, σ_{y-weld}, and the tensile yield strength of the base metal, $\sigma_{y-base-metal}$, can be considered roughly the same. The tensile yield strength of the HAZ, σ_{y-HAZ}, is considered to be roughly 15% higher than $\sigma_{y-base-metal}$. Since it is very difficult to obtain accurate shear data on materials that exhibit some ductility, very little data exist on the shear yield strength for the HAZ, $\sigma_{y-HAZ-shear}$. It is

Table 4 — ID15 Lap-Shear Data Summary

Specimen	Lap Shear Peak Load (kN)	Lap Shear Energy (Nmm)	Failure Mode
Joint ID 15 (RSW): 5182-O/6111-T4 (2 mm/2 mm)			
15LC-1	7.42	13,718.57	IF
15LC-2	7.16	9,463.15	IF
15LC-3	7.37	9,299.41	IF
15LC-4	7.33	15,359.30	IF
15LC-5	7.39	10,653.87	IF
15LC-6	7.38	9,526.16	IF
15LC-7	7.36	12,214.77	IF
15LC-8	7.12	9,877.26	IF
15LC-9	6.83	9,840.35	IF
15LC-10	6.98	9,015.96	IF
15LC-11	7.41	9,453.57	IF
15LC-12	6.61	7,600.93	IF
15LC-13	7.41	9,797.88	IF
15LC-14	6.91	7,539.23	IF
15LC-15	6.80	7,937.10	IF
15LC-16	7.28	9,111.27	IF
15LC-17	7.02	8,243.76	IF
15LC-18	7.79	11,161.31	IF
15LC-19	7.45	9,792.78	IF
15LC-20	7.24	9,715.70	IF
15LC-21	7.24	10,028.77	IF
15LC-22	7.40	9,506.06	IF
15LC-23	7.19	9,484.95	IF
15LC-24	7.10	—	IF
15LC-25	7.03	8,243.38	IF
15LC-26	7.16	8,615.48	IF
15LC-27	6.98	8,211.16	IF
15LC-28	6.71	7,349.01	IF
15LC-29	7.19	8,900.46	IF
15LC-30	6.55	7,224.97	IF
Maximum	7.79	15,359.30	
Mean	7.16	9,547.81	
Minimum	6.55	7,224.97	

Table 5 — ID15 Cross-Tension Data Summary

Specimen	Cross Tension Peak Load (kN)	Energy (Nmm)	Failure Mode	Nugget Side
	Joint ID 15 RSW: 5182-O/6111-T4 (2 mm/2 mm)			
15TC-1	5.84	54,744.00	PO	5xxx
15TC-2	6.86	61,808.00	PO	6xxx
15TC-3	6.77	61,245.00	PO	6xxx
15TC-4	6.97	67,526.00	IF-PO	6xxx
15TC-5	5.94	50,020.00	PO	5xxx
15TC-6	6.83	64,767.00	PO	5xxx
15TC-7	4.42	35,325.00	PO	5xxx
15TC-8	4.38	33,004.00	PO	6xxx
15TC-9	5.49	44,818.00	PO	5xxx
15TC-10	6.25	57,750.00	PO	6xxx
15TC-11	5.59	55,457.00	PO	6xxx
15TC-12	6.07	52,514.00	PO	6xxx
15TC-13	6.59	60,647.00	PO	5xxx
15TC-14	6.37	54,782.00	PO	5xxx
15TC-15	5.84	45,983.00	IF-PO	6xxx
15TC-16	5.05	38,761.00	PO	5xxx
15TC-17	6.22	49,426.00	PO	5xxx
15TC-18	6.53	55,274.00	PO	6xxx
15TC-19	6.65	57,700.00	PO	5xxx
15TC-20	5.50	46,349.00	PO	5xxx
15TC-21	5.29	40,516.00	PO	6xxx
15TC-22	6.10	50,830.00	PO	6xxx
15TC-23	5.91	45,109.00	PO	5xxx
15TC-24	6.88	58,865.00	PO	5xxx
15TC-25	6.03	46,745.00	PO	5xxx
15TC-26	5.39	40,903.00	PO	5xxx
15TC-27	5.25	42,237.00	PO	6xxx
15TC-28	4.92	35,422.00	IF-PO	6xxx
15TC-29	6.62	59,261.00	PO	6xxx
15TC-30	6.04	51,240.00	IF-PO	5xxx
Maximum	6.97	67,526.00		
Mean	5.95	50,634.27		
Minimum	4.38	33,004.00		

generally agreed that the shear yield strength of ductile cast iron is about 0.6 to 0.7 times its tensile yield strength (Ref. 15). Taking a similar approach, we assume here that the shear yield strength of the HAZ is about 70% of its tensile yield strength. Summarizing the above yield strength analyses, we have

$$\sigma_{y\text{–}weld} = \sigma_{y\text{–}base\text{-}metal} \quad (6)$$

$$\begin{aligned}\sigma_{y\text{–}HAZ\text{-}shear} &= 0.7 \cdot \sigma_{y\text{–}HAZ} \\ &= 0.7 \cdot 115\% \cdot \sigma_{y\text{–}base\text{-}metal} \\ &= 0.8 \cdot \sigma_{y\text{–}base\text{-}metal}\end{aligned} \quad (7)$$

Substituting Equations 6, 7, 3, and 4 into Inequality 5 produces the condition under which pullout failure mode can be ensured:

$$D_{critical} > \frac{3.2t}{f} \quad (8)$$

Therefore, for a certain sheet thickness, t, and weld porosity factor, f, the larger the weld diameter D, the better the chance for ensuring a pullout mode of failure. Also, for a certain sheet thickness, t, the lower the value f, i.e., the higher the porosity level, the larger the nugget diameter D is needed to ensure pullout failure.

The failure mode prediction methodology described above can also be illustrated schematically as shown in Fig. 16, in which the heavier lines indicate the predicted failure mode. Given a certain material thickness, t, and porosity factor, f, when D is smaller than $D_{critical}$, $F_{IF} < F_{PO}$. Therefore, interfacial fracture would be the dominant failure mode under cross tension. On the other hand, when D is greater than $D_{critical}$, $F_{PO} < F_{IF}$. Therefore, nugget pullout would be the dominant failure mode under cross-tension loading.

If one assumes f=1.0, i.e., perfect quality aluminum spot welds with no porosity and irregularity, the predicted nugget size of $3.2t$ for pullout mode can be compared

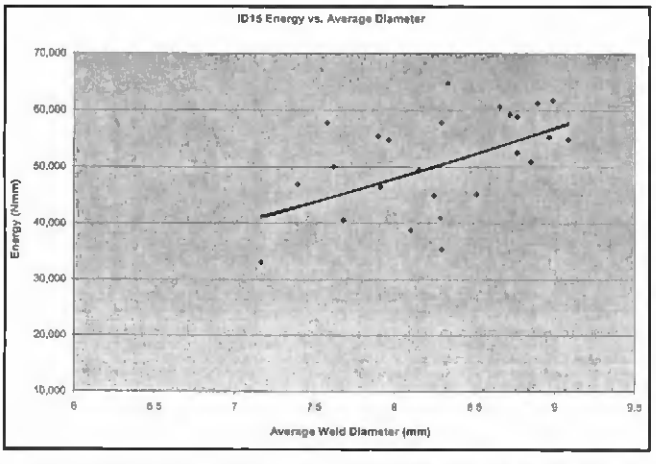

Fig. 13 — ID15 cross-tension energy absorption vs. average weld diameter.

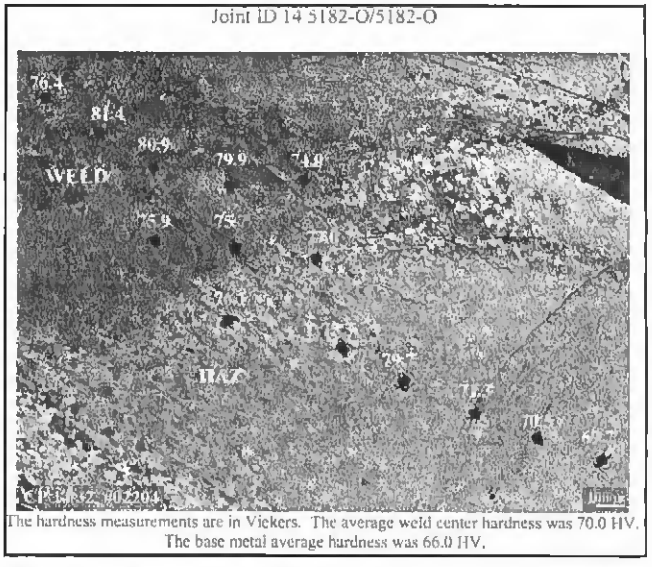

Fig. 14— Hardness traverse for ID14.

Table 6 — ID15 Coach-Peel Data Summary

Specimen	Coach Peel Peak Load (kN)	Coach Peel Energy (Nmm)	Failure Mode	Nugget Side
	Joint ID 15 RSW: 5182-O/6111-T4 (2 mm/2 mm)			
15CC-1	1.44	22,079.00	IF-PO	5xxx
15CC-2	1.28	16,117.00	PO	5xxx
15CC-3	1.51	20,058.00	IF-PO	6xxx
15CC-4	1.39	17,839.00	PO	5xxx
15CC-5	1.54	17,220.00	PO-IF	5xxx
15CC-6	1.11	15,215.00	IF-PO	6xxx
15CC-7	1.41	16,403.00	IF-PO	5xxx
15CC-8	1.27	20,466.00	IF-PO-SS	5xxx
15CC-9	1.62	33,712.00	PO	6xxx
15CC-10	1.35	23,679.00	IF-PO	6xxx
15CC-11	1.24	17,252.00	PO-IF	5xxx
15CC-12	1.26	20,947.00	PO-IF	6xxx
15CC-13	1.39	21,142.00	PO-IF	5xxx
15CC-14	1.38	19,875.00	IF-PO	5xxx
15CC-15	1.34	17,472.00	PO-IF	6xxx
15CC-16	1.25	18,398.00	IF-PO	6xxx
15CC-17	1.43	17,619.00	PO	5xxx
15CC-18	1.39	18,026.00	PO-IF	5xxx
15CC-19	1.45	24,309.00	PO-IF	5xxx
15CC-20	1.45	23,302.00	PO	6xxx
15CC-21	1.27	18,699.00	PO-IF	6xxx
15CC-22	1.42	26,706.00	PO-SS	5xxx
15CC-23	1.31	25,215.00	IF-PO	5xxx
15CC-24	1.48	20,285.00	PO-IF	6xxx
15CC-25	1.37	19,796.00	PO-IF	6xxx
15CC-26	1.38	17,241.00	PO	6xxx
15CC-27	1.40	19,160.00	PO-IF	6xxx
15CC-28	1.39	18,771.00	IF-PO	5xxx
15CC-29	1.19	17,390.00	IF-PO	6xxx
15CC-30	1.28	16,200.00	PO-IF	5xxx
Maximum	1.62	33,712.00		
Mean	1.37	20,019.77		
Minimum	1.11	15,215.00		

Table 7 — ID14 Large-Weld Cross-Tension Data Summary

Specimen	Cross Tension Peak Load (kN)	Cross Tension Energy (Nmm)	Failure Mode
14TC-31	5.8960	47,934	PO
14TC-32	3.7940	24,434	PO
14TC-33	3.7920	29,558	PO
14TC-34	3.0790	17,537	PO
14TC-35	3.6790	24,214	PO
14TC-36	6.0510	57,769	IF/PO
14TC-37	5.5320	54,446	PO
14TC-38	4.2370	34,481	PO
14TC-39	4.1860	35,231	PO
14TC-40	5.4160	45,078	PO
14TC-41	4.4860	37,030	PO
14TC-42	2.6590	15,563	PO
14TC-43	3.3660	23,930	IF/PO
14TC-44	3.8260	31,079	PO
14TC-45	5.6170	50,370	PO
14TC-46	4.7980	44,482	PO
14TC-47	3.1540	20,415	PO
14TC-48	5.2200	52,467	PO
14TC-49	6.4430	66,594	PO
14TC-50	6.4450	64,080	PO
14TC-51	6.6860	79,861	PO
14TC-52	3.8140	38,295	PO
14TC-53	2.6400	16,322	PO
14TC-54	3.5170	27,666	PO
14TC-55	3.2680	24,078	PO
14TC-56	4.5170	42,731	PO
14TC-57	5.9270	61,015	PO
14TC-58	5.4690	60,233	PO
14TC-59	6.5870	63,327	PO
14TC-60	5.7880	54,103	PO
Maximum	6.6860	79,861.00	
Mean	4.6630	41,477.43	
Minimum	2.6400	15,563.00	

with the conventional recommended minimal nugget size of $4\sqrt{t}$. If the thickness of the aluminum sheet being welded is less than 1.5625 mm, then the conventional minimal nugget size recommendation of $4\sqrt{t}$ is sufficient to ensure nugget pullout. On the other hand, if the aluminum sheet thickness is greater than 1.5625 mm, the recommended minimal nugget size of $4\sqrt{t}$ is smaller than $3.2t$. Therefore, the recommended minimal weld size of $4\sqrt{t}$ is not sufficient to ensure nugget pullout failure under cross-tension loading condition. If one were to take into consideration weld porosity and irregularity of the actual production welds, the nugget size needs to be further increased to ensure nugget pullout.

From another perspective, Fig. 16 also indicates that the cross-tension strength of the weld depends primarily on the weld diameter D under a certain level of porosity. For weld diameters smaller than $D_{critical}$, interfacial fracture failure mode would be dominant, and the peak failure load would increase in a parabolic fashion with respect to the weld diameter. For weld diameters greater than $D_{critical}$, nugget pullout would be the dominant failure mode, and peak failure load increases linearly with the weld diameter. This conclusion validates the observations obtained in the previous section on the effect of weld size. It is also consistent with the observations reported in Ref. 12, which stated that weld size is an influencing factor in determining the different failure modes for spot welds of 6XXX series of aluminum alloys.

Model Validation and Discussions

In order to validate the above analytical failure mode model, two additional populations of aluminum spot welds with 2-mm AA5182-O were fabricated for cross-tension loading condition. Our intention was to make one sample population with a weld size smaller than the original ID14, and another sample population with a weld size larger than ID14. We labeled these populations as ID14-small-weld and ID14-large-weld. The intended fusion zone diameter for the ID14-small-weld population was 5.5 to 6.1 mm, and the intended fusion zone size for the ID14-large-weld population was 9 to 10.6 mm. Typical weld cross sections for ID14-small-weld and ID14-large-weld are shown in Fig. 17. Note that the small weld population has the desired weld size of $4\sqrt{t}$ (Ref. 9). Again, 30 replicates of quasistatic cross-tension tests were conducted for each population, and the resulting peak load and joint failure modes were recorded.

According to Figs. 4 and 17, the area percentage of porosity on the faying interface can be estimated as ~15 to 20% for a typical weld in ID14, ID14-small-weld, and ID14-large-weld. Assuming the same level of f=0.85 for all three populations, we derive $D_{critical}$ =7.5 mm according to Equation 8 for 2-mm AA5182-O sheet. Since the weld sizes for the samples in ID14 were controlled to be around 8 mm, this may explain why the majority of the cross-tension samples in ID14 failed in nugget pullout mode. The recorded

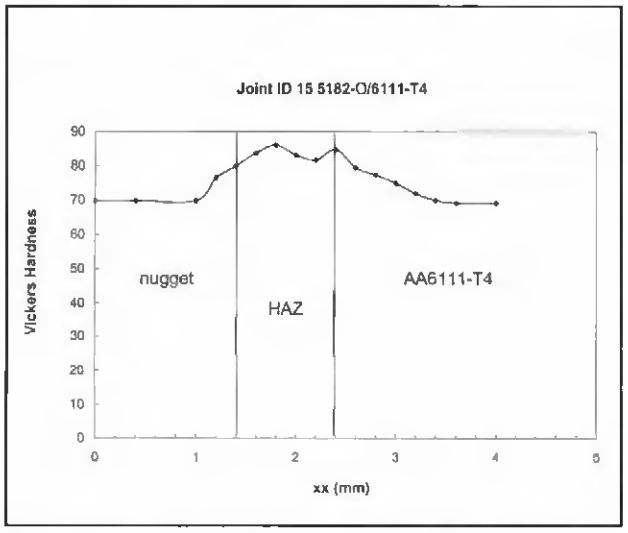

Fig. 15 — ID15 Vickers hardness measurement. The test force applied was 100 gf.

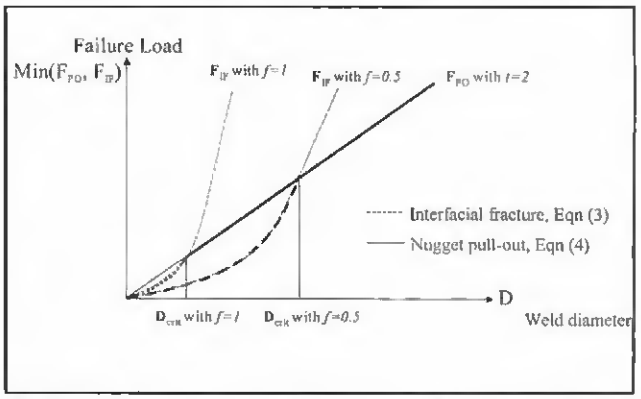

Fig. 16 — Schematic illustration of cross-tension failure load and failure mode vs. weld diameter under different porosity levels.

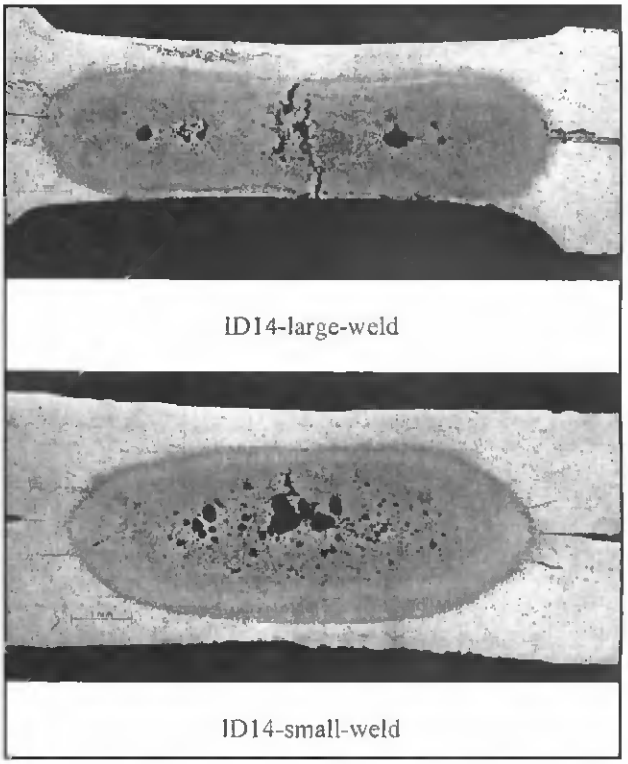

Fig. 17 — Typical metallurgical cross sections for ID14-large-weld and ID14-small-weld.

nugget sizes shown in Figs. 10 and 11 also confirm that all the welds in ID14 that failed in nugget pullout mode have weld diameters greater than 7.5 mm.

Furthermore, when we increased the weld size to 9–10 mm as in population ID14-large-weld, 28 out of the 30 welds tested failed in nugget pullout mode. See Table 7 for the summary of failure mode and nugget size for this population. The two welds that failed in interfacial fracture mode have irregular fusion zone shape, and their minimum fusion zone diameters are measured to be 4.95 and 7.1 mm, respectively.

For ID14-small-weld population, 22 out of the 30 welds tested failed in interfacial fracture mode and 8 welds failed in nugget pullout mode (Table 8). The actual fusion zone size for ID14-small-weld is larger than its intended value, with average fusion zone size around 7.1 mm. Since their average diameter is lower than the predicted critical value, the majority of the welds failed in interfacial fracture mode.

Figure 18 summarizes the experimentally observed failure modes for the original ID14, ID14-small-weld, and ID14-large-weld populations. The dominant failure modes for the three populations change from interfacial fracture to nugget pullout with increasing fusion zone size. Considering the statistical nature of weld size, porosity level, and distribution, the analytical model works reasonably well in predicting the critical weld size for nugget pullout.

Thus far, we have validated Equation 8 on the effect of fusion zone size D for fresh welds with consistent porosity levels. The validations do not include the effects of weld porosity factor f. Since the level of weld porosity and its distributions are closely related to electrode wear (Ref. 18), further validations on the effect of porosity factor f should be investigated in conjunction with studies on electrode wear.

It is worth noting that given the material properties and the nugget size, one can also use Equations 3, 4, 6, and 7 to quickly estimate the anticipated cross-tension strength of a spot weld population. For example, the shear strength of AA5182-O used in ID14 and ID15 is about 140 MPa according to Refs. 16 and 17. Given the sheet thickness of 2 mm and the average nugget size of 8.5 mm, Equation 4 estimates the weld pullout strength to be

$$F_{PO} = \pi \cdot D \cdot t \cdot \sigma_{y-HAZ-shear} \approx \pi \cdot 8.5 \cdot 2 \cdot 0.8 \cdot 140 = 5.98\ kN \quad (9)$$

The estimated cross-tension strength in Equation 9 is very close to the strength data reported in Tables 2 and 5.

As noted in Equation 4, the actual weld pullout strength under cross-tension loading condition also depends on the degree of weld indentation. Therefore, the facts that a weld has a larger fusion zone diameter and that it fails in nugget pullout mode cannot guarantee it is stronger than a weld with a smaller fusion zone for the same material combination. An example of this is shown in Fig. 19 with the peak loads of ID14, ID14-small-weld, and ID14-large-weld compared. Even though ID14-large-weld has a larger fusion zone size than ID14, its average static strength is lower than that of ID14 because of its severe weld indentation and, therefore, the reduced effective sheet thickness t (see Fig. 17).

Another interesting observation from Fig. 19 is that, for joint ID14-small-weld, the mean strength for the samples that failed in interfacial fracture mode is considerably lower than that of the samples

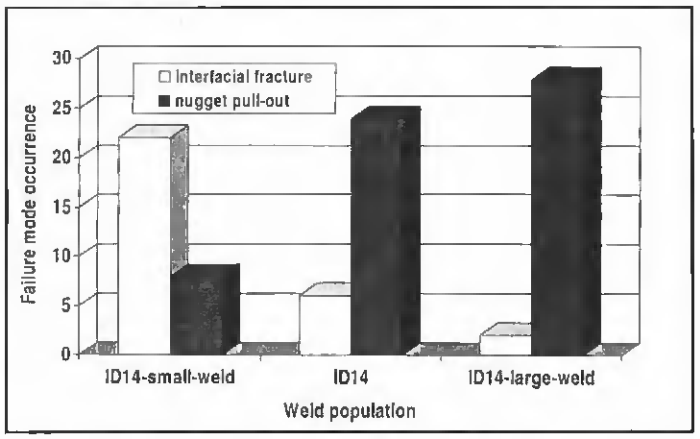

Fig. 18 — Comparison of failure modes vs. weld fusion zone size.

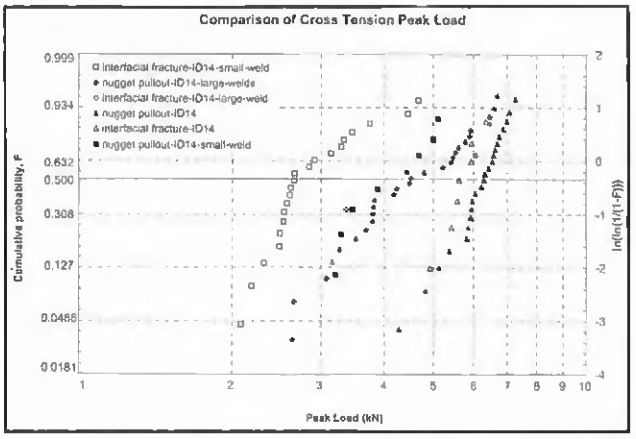

Fig. 19 — Comparison of cross-tension peak load distributions for ID14, ID14-large-weld, and ID14-small-weld.

that failed in nugget pullout mode. With increasing fusion zone sizes for ID14 and ID14-large-weld, the strength differences between the two failure modes decrease. Therefore, the observations we made earlier on the effects of failure modes on peak load and energy absorption for ID14 and ID15 cannot be generalized to welds with fusion zone size smaller than $D_{critical}$. In addition, for the population ID14-large-weld, the samples that failed in interfacial fracture mode have a similar level of median strength, but a larger level of scatter than those that failed in nugget pullout mode.

It should also be noted that even though the analytical part of the study focuses on aluminum spot welds, a similar analysis procedure may also be used for spot welds of ultrahigh-strength steel because of the similar characteristics of the hardness traverse plots. For both of these materials, the weld nugget does not have significantly higher yield strength than the base metal and the heat-affected zone. Moreover, based on a similar microhardness argument, it can be shown that the traditional criterion for rejecting interfacial fracture welds works well in evaluating the quality of mild-steel spot welds.

Conclusions

Through experimental investigation, statistical study, and analytical study, the following conclusions can be derived from this research:

Theoretically, weld size, sheet thickness, and level of weld porosity are the main factors determining the cross-tension failure mode for the aluminum spot welds studied in this paper. For a given sheet thickness and porosity level, the larger the weld size in comparison with $D_{critical}$, the more likely the weld will fail in nugget pullout mode under cross tension. It should be noted that this conclusion is quantitatively valid for situations where the weld metal and HAZ hardness/strength are similar to those of the base metal. If substantial strength disparities exist (e.g., when welding precipitation-hardening alloys in the T6 condition), the critical weld diameter for pullout failures could be significantly shifted according to Equations 3 and 4.

For the two populations of aluminum spot welds in ID14 and ID15, different failure modes under cross-tension and coach peel loading conditions do not significantly influence the static peak load and energy absorption levels of the samples. In a statistical sense, the pullout mode generates less than 10% higher peak load and total energy absorption compared with the interfacial fracture mode. However, this conclusion cannot be generalized to weld populations with fusion zone sizes smaller than $D_{critical}$.

For the cross-tension samples that failed in nugget pullout mode in ID14 and ID15, larger weld diameter generates higher peak load and higher energy absorption.

Severe weld indentation reduces the static strength of cross-tension samples. In general, if we consider two samples from two different weld populations, the sample with larger weld size does not guarantee higher cross-tension strength even when both samples fail in nugget pullout mode. The degree of weld indentation should also be considered.

The cross-tension strength of aluminum welds can be reasonably estimated given the material's yield strength, sheet thickness, weld size, and the level of weld porosity.

The conclusions of this study seem to suggest that one would want to increase the weld size indefinitely to achieve a higher level of peak load and energy absorption. Practically, larger weld size is also associated with a higher energy requirement for the welding equipment, faster electrode wear, and possible weld indentation. Therefore, the optimized value of weld size should be selected based on practicality and fitness-for-service criteria.

Table 8 — ID14 Small-Weld Cross-Tension Data Summary

Specimen	Cross Tension Peak Load (kN)	Energy (Nmm)	Failure Mode
14TC-24	No Test		—
14TC-1	4.68	31,033	IF
14TC-11	2.09	8,434	IF/PO
14TC-5	2.19	15,579	IF/PO
14TC-9	2.32	12,622	IF/PO
14TC-4	2.48	14,118	IF/PO
14TC-18	2.49	12,211	IF/PO
14TC-2	2.53	12,013	IF/PO
14TC-6	2.53	12,200	IF/PO
14TC-29	2.57	16,894	IF/PO
14TC-14	2.60	13,491	IF/PO
14TC-19	2.62	19,329	IF/PO
14TC-20	2.66	15,964	IF/PO
14TC-7	2.66	15,321	IF/PO
14TC-17	2.84	16,907	IF/PO
14TC-3	2.91	15,622	IF/PO
14TC-21	3.15	23,813	IF/PO
14TC-16	3.29	23,158	IF/PO
14TC-22	3.33	20,740	IF/PO
14TC-10	3.46	27,209	IF/PO
14TC-13	3.75	30,792	IF/PO
14TC-8	4.46	38,571	IF/PO
14TC-27	3.20	25,993	PO
14TC-26	3.29	26,710	PO
14TC-30	3.46	26,788	PO
14TC-25	3.88	31,477	PO
14TC-12	4.44	34,168	PO
14TC-28	4.69	45,410	PO
14TC-15	5.00	44,041	PO
14TC-23	5.11	46,097	PO
Maximum	5.11	46,097.00	
Mean	3.26	23,334.66	
Minimum	2.09	8,434.00	

Acknowledgments

Pacific Northwest National Laboratory is operated by Battelle for the U.S. Department of Energy (DOE) under Contract DE-AC06-76RL01830. The DOE FreedomCAR and Vehicle Technologies funded this work. The DOE program manager is Dr. Joseph Carpenter, and the USCAR program manager is James Quinn.

Fruitful technical discussions with James Dolfi of Dolfi AWS LLC are also gratefully acknowledged.

References

1. Chuko, W. L., and Gould, J. E. 2002. Development of appropriate resistance spot welding practice for transformation-hardened steels. *Welding Journal* 81(1): 1-s to 7-s.

2. Perterson, W. 1997. Dilution of weld metal to eliminate interfacial fractures of spot welds in high and ultrahigh-strength steels. Columbus, Ohio: ICAWT.

3. Riesner, M., Sun, X., Wu, S., Hwang, H. Y., and Low, E. 2000. Modeling and optimization of structural joints in automotive applications. *Proceedings of the International Crashworthiness Conference*. London, Sept. 4–7. 2000. Paper No. 2096.

4. Browne, D. J., Chandler, H. W., Evans, J. T., and Wen, J. 1995. Computer simulation of resistance spot welding in aluminum: Part I. *Welding Journal* 74(10): 339-s to 344-s.

5. Browne, D. J., Chandler, H. W., Evans, J. T., James, P. S., Wen, J., and Newton, C. J. 1995. Computer simulation of resistance spot welding in aluminum: Part II. *Welding Journal* 74(12): 417-s to 422-s.

6. Spinella, D. J., Otteren, R. V., Borenik, B., and Patrick, E. P. 2000. Single-sided projection welding of aluminum automotive sheet using the HY-PAK® welding process. SAE paper No. 2000-01-2678.

7. Sun, X. and Dong, P. 2000. Analysis of aluminum resistance spot welding processes using coupled finite element procedures. *Welding Journal* 79(8): 215-s to 221-s.

8. Sun, X., Dong, P., and Kimchi, M. 1997. The coupled electrical-thermal-mechanical process associated with aluminum RSW. *Proceedings of the Seventh International Conference on Computer Technology in Welding*. Ed. T. Siewert, pp. 447–457.

9. *Weld Quality Test Method Manual*. Standardized Welding Test Method Task Force, Auto/Steel Partnership, October 1997.

10. Ang, A. H-S., and Tang, W. H. *Probability Concepts in Engineering Planning and Design*, Vol. 1, Basic Principles. New York: John Wiley & Sons.

11. Khaleel, M. A., and Saunders, S. C. 1997. On the fatigue-life distributions of engineering materials. *International Journal of Reliability, Quality and Safety Engineering* 4(1): 93–115.

12. Spinella, D. J. 2002. 6xxx series aluminum alloys weld lobe study. ALCOA private communications.

13. Lin, S.-H., Pan, J., Wu, S.-R, Tyan, T., and Wung, P. 2002. Failure loads of spot welds under combined opening and shear static loading conditions. *International Journal of Solids and Structures* 39(2002): 19–39.

14. Zhou, M., Hu, S. J., and Zhang, H. 1999. Critical specimen sizes for tensile-shear testing of steel sheets. *Welding Journal* 78(9): 305-s to 313-s.

15. *Metals Handbook*, Ninth Edition, Vol. 1. Properties and Selection: Irons and Steels. 1978. Metals Park, Ohio: ASM International.

16. *ASM Specialty Handbook: Aluminum and Aluminum Alloys*. 1993. Metals Park, Ohio: ASM International.

17. Fukumoto, S. Lum, I. Biro, E., Boomer, D. R., and Zhou, Y. 2003. Effects of electrode degradation on electrode life in resistance spot welding of aluminum Alloy 5182. *Welding Journal* 82(11): 307-s to 312-s.

18. Chuko, W., and Gould, J. 2000. Metallurgical interpretation of electrode life behavior in resistance spot welding of aluminum sheet. *Proc. Joining of Advanced and Specialty Materials*, Oct. 9–11, 2000. St. Louis, Mo., ASM International, pp. 114–121.

Preparation of Manuscripts for Submission to the *Welding Journal* Research Supplement

All authors should address themselves to the following questions when writing papers for submission to the Welding Research Supplement:

- Why was the work done?
- What was done?
- What was found?
- What is the significance of your results?
- What are your most important conclusions?

With those questions in mind, most authors can logically organize their material along the following lines, using suitable headings and subheadings to divide the paper.

1) **Abstract.** A concise summary of the major elements of the presentation, not exceeding 200 words, to help the reader decide if the information is for him or her.

2) **Introduction.** A short statement giving relevant background, purpose, and scope to help orient the reader. Do not duplicate the abstract.

3) **Experimental Procedure, Materials, Equipment.**

4) **Results, Discussion.** The facts or data obtained and their evaluation.

5) **Conclusion.** An evaluation and interpretation of your results. Most often, this is what the readers remember.

6) **Acknowledgment, References and Appendix.**

Keep in mind that proper use of terms, abbreviations, and symbols are important considerations in processing a manuscript for publication. For welding terminology, the *Welding Journal* adheres to AWS A3.0:2001, *Standard Welding Terms and Definitions*.

Papers submitted for consideration in the Welding Research Supplement are required to undergo Peer Review before acceptance for publication. Submit an original and one copy (double-spaced, with 1-in. margins on 8 ½ x 11-in. or A4 paper) of the manuscript. A manuscript submission form should accompany the manuscript.

Tables and figures should be separate from the manuscript copy and only high-quality figures will be published. Figures should be original line art or glossy photos. Special instructions are required if figures are submitted by electronic means. To receive complete instructions and the manuscript submission form, please contact the Peer Review Coordinator, Doreen Kubish, at (305) 443-9353, ext. 275; FAX 305-443-7404; or write to the American Welding Society, 550 NW LeJeune Rd., Miami, FL 33126.